Effect of dimple offset on the operational shock performance of small form factor disk drives

Puneet Bhargava and David B. Bogy

Computer Mechanics Laboratory

Department of Mechanical Engineering

University of California at Berkeley

Berkeley, CA 94720

Telephone: (510) 642-4975

Fax: (510) 643-9786

puneet@cml.berkeley.edu

December 5, 2006

Contents

List of Figures

List of Tables

Abstract

This paper discusses the effect of varying the location of the load dimple on the suspension on the shock response of small form factor hard disk drives. We use the CML shock simulator, which simulates the structural as well as the air bearing dynamics of the disk drive simultaneously. The location of the dimple is varied and simulations are run for various load positions on the back of the slider, while adjusting the pitch static attitude (PSA) and the roll static attitude (RSA) of the slider such that the flying attitude of the slider remains the same. We simulate shocks of 0.5 ms pulse width for a commercially available slider and suspension designs for a 1" drive. We observe that shock resistance is optimal when the dimple is offset towards the leading edge of the slider. This behavior is explained on the basis of a linearized air bearing model. It is also observed that moving the dimple too much towards the leading edge causes the mechanism of shock failure to change resulting in lower shock tolerances.

1 Introduction

1.1 Motivation

Recently there has been an increased interest in the effect of shocks on hard disk drives due their usage in more hostile environments. Over the past few years an increase in the demand of storage capacity in small consumer appliances and gadgets such as MP3 players, cameras and cell phones has led to the application of small form factor hard disk drives in these devices. Due to the hostile environments faced by such devices, the shock resistance of these small form factor drives has become of great importance.

1.2 Methodology

In this paper we study the effect of varying the location of the dimple (pivot) of the suspension on the shock performance of a small form factor drive. Previously we have developed a shock

simulator to accurately simulate the shock event and predict the response of the suspension-slider-disk system (Bhargava and Bogy (2005a)). This simulator is used to simulate the shock response of a system for a suspension system with varying dimple locations in the x and y directions (see Fig.1. Simulations are carried out to determine the 'safe' operating shock levels, wherein no head-disk contacts occur.

1.3 Prior Work

Over the past few years there have been various experimental and simulation studies on the shock response of the hard disk drive mechanical system and its effects on the head-disk interface. Many of these studies (Harrison and Mundt (2000), Edwards (1999), Kumar et al. (1994), Kouhei et al. (1995)) have been limited to the non-operating state of the drives, and/or to the component level. Various other papers (Jayson et al. (2003), Jiang et al. (1995)) have considered shock simulations in the operating state using simplified models for one or more components of the drive, i.e. either the disk, suspension or the air bearing. A summary of these studies has been presented in Bhargava and Bogy (2005b).

For the simulation of operational shock Zeng and Bogy (2000) proposed a method whereby they separate the simulation work into two essentially uncoupled sets. They developed a finite element model of the disk and suspension system and used it to obtain the dynamic normal load and moments applied to the slider air bearing. These were then used as input data for an air bearing dynamic simulator to calculate the dynamic flying attitudes. They were able to obtain not only the responses of the structural components, but also the responses of the slider air bearings. Also, simulations where the air bearing exhibits highly nonlinear behavior, such as when the air bearing collapses, may require iterations between the structural and air bearing simulations, thereby making the process cumbersome and computationally more expensive. In a previous paper, Bhargava and Bogy (2005a) proposed a method where the structural modeling module is transferred into the air bearing code using preassembled exported mass and stiffness matrices from ANSYS. This method was found to

be accurate, fast and robust. The authors simulated the effect of the pulse width on the shock resistance of a 1" drive.

In this paper, we study the effect of the load dimple location, on the shock performance of a small form factor drive. For such an application it is critical to accurately model the suspension, as well as the nonlinear behavior of the dimple due to contact.

2 Simulations

2.1 Procedure

The new CML Dynamic Load/Unload/Shock simulator (Bhargava and Bogy (2006)) is used to simulate the shock response of a commercially available 1" drive slider and suspension design while varying the location of the dimple. We determine the 'safe' shock levels for each location, as the maximum shock amplitude for which no head-disk contacts are observed. Bhargava and Bogy (2005b) defined two types of shocks, namely positive and negative (where the acceleration pulse is applied in the $+z$ and $-z$ directions respectively). They also showed that drive are less robust for positive shocks than for negative shocks. In another report (Bhargava and Bogy (2005a)), the authors demonstrated that the mechanism of failure for shocks with pulse widths in the range of 0.5 ms to 3.0 ms is similar. Hence, in this study we simulate only positive shocks with pulse width 0.5 ms.

Figure 2 shows a schematic diagram of a suspension. A typical suspension consists of a slider mounted on a flexure. The flexure provides roll and pitch stiffness to the slider, while the stiffness in the z direction is provided by the load beam through a dimple which pushes down into the flexure that adheres to the slider. Limiters may be provided on the suspension to limit the maximum separation of the flexure from the dimple during unloading. Figure 3 shows a free body diagram of the slider in the steady state flying condition. For simplicity, we consider here the force and moment balances in the $z - x$ plane only. Forces and moments in the third direction can be similarly balanced. We also assume that the gram

load on the slider is completely applied by the dimple and moments are applied only by the flexure, thereby neglecting the z-stiffness of the flexure and the friction moments applied by the dimple. Writing the force balance in the z-direction and the moments in the y-direction, we have,

$$F_b = F_g \tag{1}$$

$$M_f - F_g \times x_l = M_b \tag{2}$$

Thus to get the same torques in the steady state (and hence the same flying attitude for the slider) for different load points x_l, the $F_g x_l$ term needs to be balanced by the M_f term, which is achieved by adjusting the PSA of the slider to generate the additional moment. If x_l is positive, a negative PSA is used, and vice versa. Similarly in the $z-y$ plane, the RSA is adjusted to maintain the same flying roll attitude.

2.2 Results and Analysis

We carried out simulations for various dimple locations on the flexure for half sinusoid shocks of varying magnitudes. The operating parameters of the slider used are listed in Table 1.

Figure 4 presents several graphs of the shock response to a 0.5 ms pulse width for the dimple located at the centre of the slider (BC) ($x_l = 0.0$,$y_l = 0.0$) mm). In Fig. 5, we plot the dimple separation and dimple contact forces. It is observed that during the course of the shock, the load beam is pulled up and the dimple separates from the flexure. Subsequently, the load beam slaps back onto the flexure, hitting it with a large contact force. This causes the slider to crash into the disk. This kind of response is typical for shock pulse widths of 0.5 ms. The mechanism of failure has been previously shown to be typical of pulse widths of 0.5 - 3.0 ms (Bhargava and Bogy (2005a)).

Figure 6 shows the shock response for the dimple location U1 ($x_l = -0.1$,$y_l = 0.0$ mm). We observe no head disk contact in this case. In Fig. 7 we plot the dimple separation, as

well as the dimple contact force. As the dimple unloads, we observe in Fig. 6f that the pitch angle is larger than was observed for the base case (BC) in Fig. 4. This is a consequence of the positive PSA used to account for the dimple load moment $F_g x_l$. We also note that the minimum fly height is less than what was observed for the base case, again as a consequence of the larger pitch angle. As the load beam snaps back onto the flexure, there is a spike in the dimple contact force. This large contact force also generates a contact moment about the centre of the slider.

We can explain this difference in the behavior of the two dimple location cases using a simple linearized dynamic model.

Here, z is the fly height of the centre of the slider, α is the pitch and β is the roll of the slider. We linearize the air bearing for the base case at time t, with attitude $\mathbf{u_0}$ which is the instant when the load beam impacts the flexure (see Fig. 8). The incremental force vector F defined as the vector of restoring forces and moments generated due to changes in the attitude, is given by:

$$\mathbf{F} = \mathbf{K_b u}, \tag{3}$$

where the attitude vector $\mathbf{u}$ and force vector $\mathbf{F}$ are defined as:

$$\mathbf{u} = \left\{ \begin{array}{c} z \\ \alpha \\ \beta \end{array} \right\}; \mathbf{F} = \left\{ \begin{array}{c} F_z \\ M_\alpha \\ M_\beta \end{array} \right\} \tag{4}$$

The matrix $\mathbf{K_b}$ is the linear spring stiffness of the air bearing, given as:

$$\mathbf{K_b} = \left\{ \begin{array}{ccc} k_{zz} & k_{z\alpha} & k_{z\beta} \\ k_{\alpha z} & k_{\alpha\alpha} & k_{\alpha\beta} \\ k_{\beta z} & k_{\beta\alpha} & k_{\beta\beta} \end{array} \right\} \tag{5}$$

Inverting the stiffness matrix, we obtain the compliance matrix, which relates the attitude

of the slider to applied forces and moments.

$$\mathbf{C} = \mathbf{K_b}^{-1} \tag{6}$$

$$\mathbf{u} = \mathbf{CF} \tag{7}$$

We observe that during head-disk contact, the pitch is positive, while the roll can be positive or negative depending on the value of y_l, slider design, skew and other operating parameters. Thus the location of the point on the slider with the minimum fly height will be near the trailing edge. For simplicity, we can assume that the minimum fly height (z_{min}) location is infact one of the corners of the trailing edge (depending on the roll of the slider). Then we calculate the ratio of the displacement of the minimum fly height to an applied force at (x_l, y_l), i.e. $c_{z_{min}G)}$. A force F_g acting at (x_l, y_l) is equivalent to the following force vector in our defined attitude coordinate system:

$$\mathbf{F} = \left\{ \begin{array}{c} F_g \\ F_g x_l \\ F_g y_l \end{array} \right\} \tag{8}$$

Also we can calculate z_{min}, given the slider attitude vector as:

$$z_{min} = \left\{ \begin{array}{ccc} 1 & \frac{l}{2} & sign(\beta)\frac{b}{2} \end{array} \right\} \left\{ \begin{array}{c} z \\ \alpha \\ \beta \end{array} \right\} \tag{9}$$

Here l and b are the length and breadth of the slider, and the pitch and roll are assumed to be small. Thus we have for $c_{z_{min}G}$:

$$c_{z_{min}G} = \left\{ \begin{array}{ccc} 1 & \frac{l}{2} & \frac{b}{2} \end{array} \right\} \mathbf{C} \left\{ \begin{array}{c} F_g \\ F_g x_l \\ F_g y_l \end{array} \right\} \tag{10}$$

The $c_{z_{min}G}$ values for various values of x_l and y_l have been plotted in Fig. 9 using K_b determined from simulations for our system. The black line on the plot is the zero displacement line, which means that the minimum fly height will not change when a small force is applied in the z direction anywhere along this line. This concept is similar to a 'center of percussion', the only difference being that we are looking at the displacement of a point other than where the force is applied. A positive value of $c_{z_{min}G}$ implies that the change in the minimum fly height will be positive for a given positive F_g applied at (x_l, y_l), while a negative value indicates that the minimum fly height will actually increase when a force F_g is applied at (x_l, y_l). We see that $c_{z_{min}G}$ is smallest when $x_l = \frac{l}{2}$ and $y_l = \pm\frac{b}{2}$. However, earlier we noted that the pitch for the U1 case was larger than, and the minimum fly height was lower than, that of the BC, before the load beam had snapped back onto the flexure. If we choose a large negative value of x_l, the slider crashes into the disk even before the load beam snaps back onto the flexure. In Fig. 10 we plot the flying attitude for location U2 ($x_l = -0.2, y_l = 0.0$) mm). We observe that the mechanism of failure for this dimple location is completely different from that in the first two cases. In Fig. 11 we plot the dimple separation and contact force. We see that the slider crashes soon after the dimple separates. This is due to the large positive torque generated as the dimple unloads.

Various other simulations were carried out at other values of (x_l, y_l) to determine the 'safe' shock map shown in Fig. 12 for this particular slider-suspension system.

3 Conclusions

The effect of the location of the dimple on the shock performance of a small form factor drive was investigated. Simulations were carried out using the CML Dynamic L/UL/S simulator using a shock pulse. The results of the study are summarized in Fig. 12. We see that maximum shock resistance is realized when the dimple is located at $(-0.13, 0.015)$. It was shown that moving the dimple towards the leading edge of the slider improves shock performance when the mechanism of shock failure is load beam-flexure impact. However if the dimple is moved too far, the mechanism of shock failure changes and shock performance degrades.

Acknowledgment

This study was supported by Seagate Corporation and the Computer Mechanics Laboratory (CML) at the University of California, Berkeley.

References

P. Bhargava and D. B. Bogy. Effect of shock pulse width on the shock response of small form factor disk drives. Technical Report 2005-018, CML, University of California, Berkeley, 2005a.

P. Bhargava and D. B. Bogy. Numerical simulation of operational-shock in small form factor hard disk drives. Technical Report 2005-005, CML, University of California, Berkeley, 2005b.

P. Bhargava and D. B. Bogy. The cml dynamic load/unload/shock simulator (v 5.1). Technical Report 2006-009, CML, University of California, Berkeley, 2006.

J. R. Edwards. Finite element analysis of the shock response and head slap behavior of a hard disk drive. *IEEE Trans. of Magnetics*, 35:863–867, 1999.

J. C. Harrison and M. D. Mundt. Flying height response to mechanical shock during operation of a magnetic hard drive. *ASME Journal of Tribology*, 122:260–263, 2000.

E. M. Jayson, J. Murphy, P. W. Smith, and F. E. Talke. Shock modeling of the head-media interface in an operational hard disk drive. *IEEE Trans. of Magnetics*, 39:2429–2432, 2003.

Z. W. Jiang, K. Takashima, and S. Chonan. Shock proff design of head disk assembly subjected to impulsive excitation. *JSME International Journal*, 38:411–419, 1995.

T. Kouhei, T. Yamada, Y. Keroba, and K. Aruga. A study of head-disk interface shock resistance. *IEEE Trans. of Magnetics*, 31:3006–3008, 1995.

S. Kumar, V. Khanna, and M. Sri-Jayantha. A study of the head disk interface shock failure. In *The 6th MMM-Intermag Conference*, 1994.

Q. Zeng and D. B. Bogy. Numerical simulation of shock response of disk-suspension-slider

air bearing systems in hard disk drives. Technical Report 2000-003, CML, University of California, Berkeley, 2000.

4 Tables

Table 1: Slider parameters

Parameter	Value
Drive form factor	1”
Gram load	1.25 g
RPM	3600
Steady state flyheight (OD)	6.24 nm
Steady state pitch	58.3 μrad
Steady state roll	-2.6 μrad
Operating PSA	2.5 mrad
Operating RSA	0.0 mrad

5 Figures

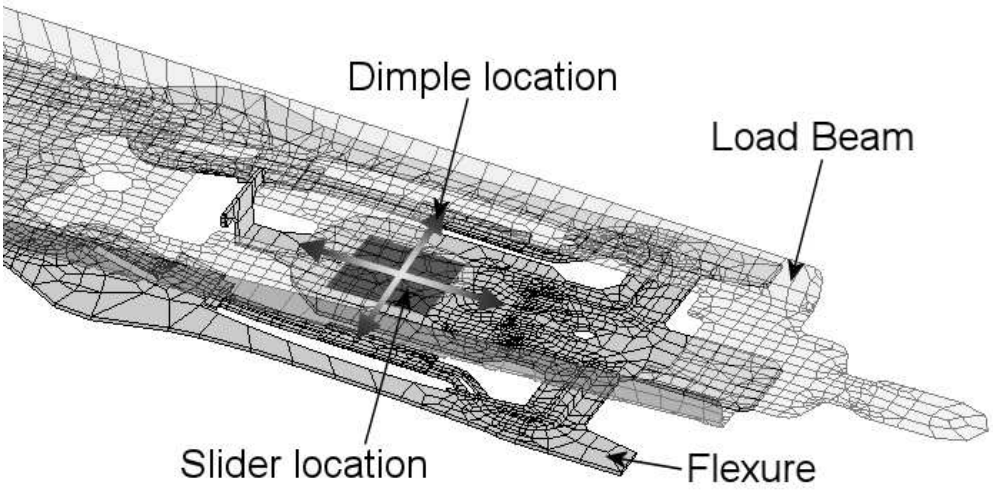

Figure 1: Suspension system

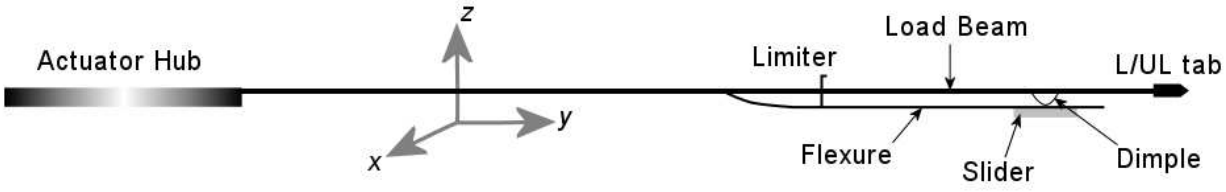

Figure 2: Suspension schematic

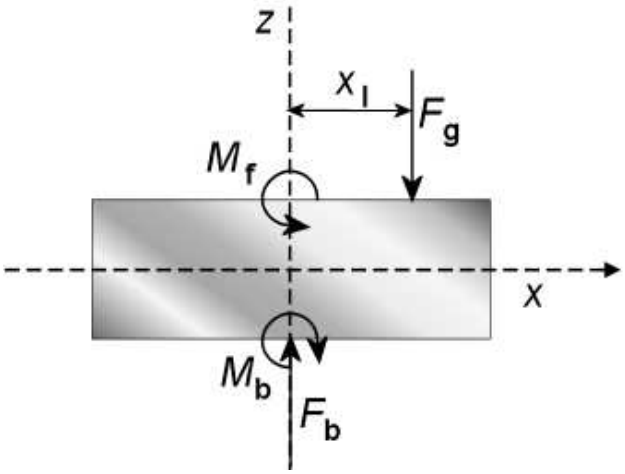

Figure 3: Slider free-body diagram

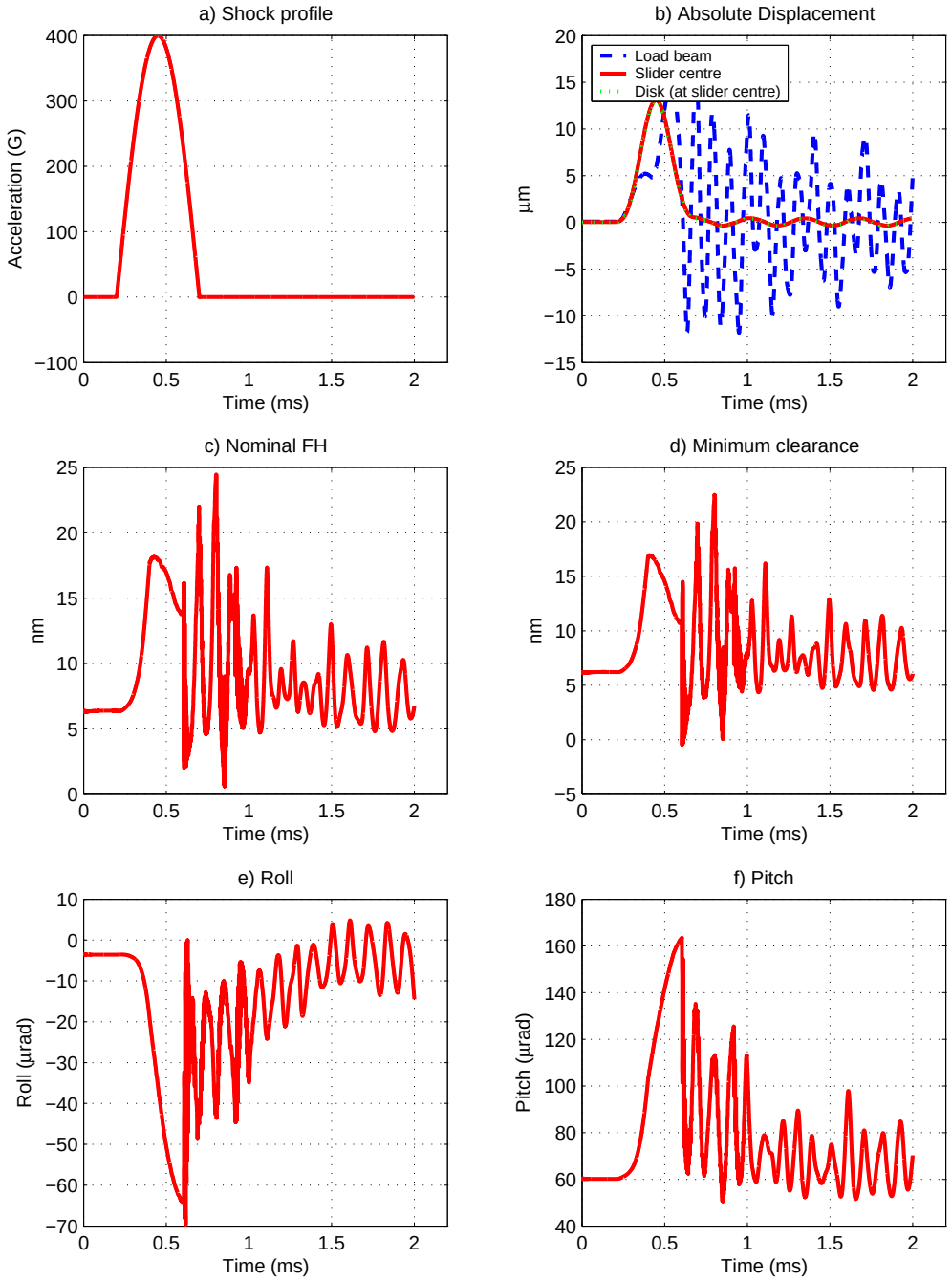

Figure 4: Slider attitude for BC 400G shock

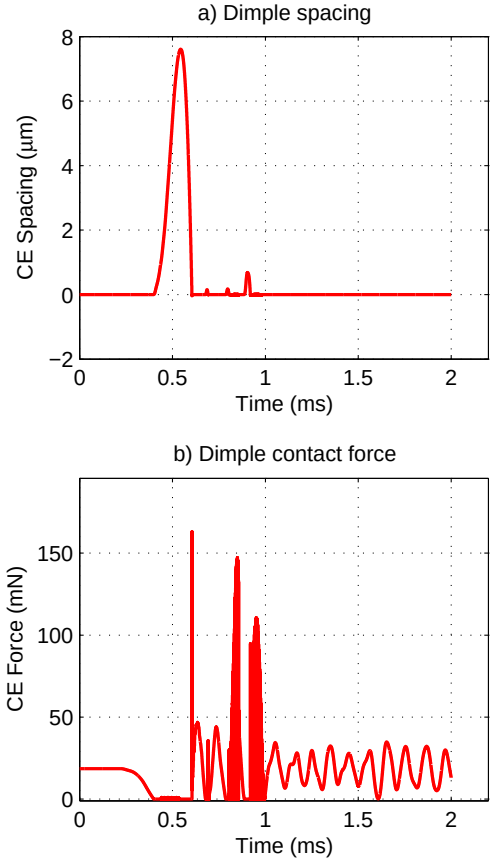

Figure 5: Dimple separation and contact force for BC 400G shock

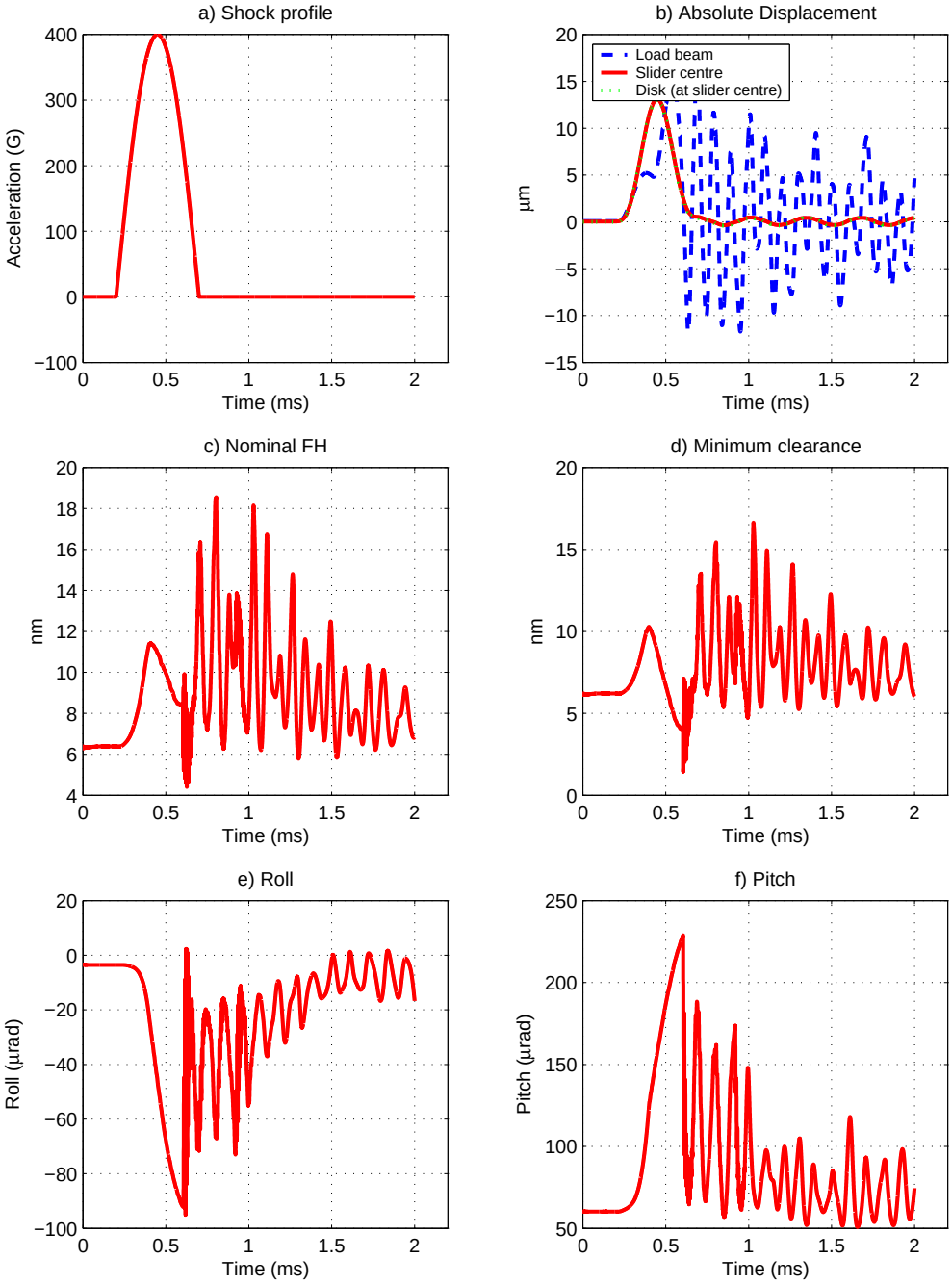

Figure 6: Slider attitude for U1 400G shock

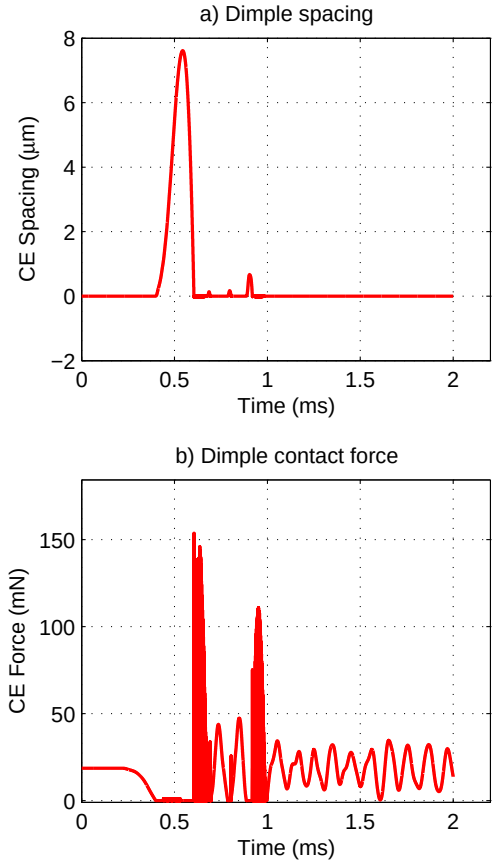

Figure 7: Dimple separation and contact force for U1 400G shock

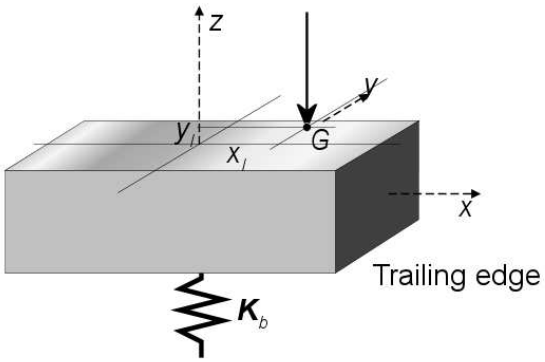

Figure 8: Linearized system

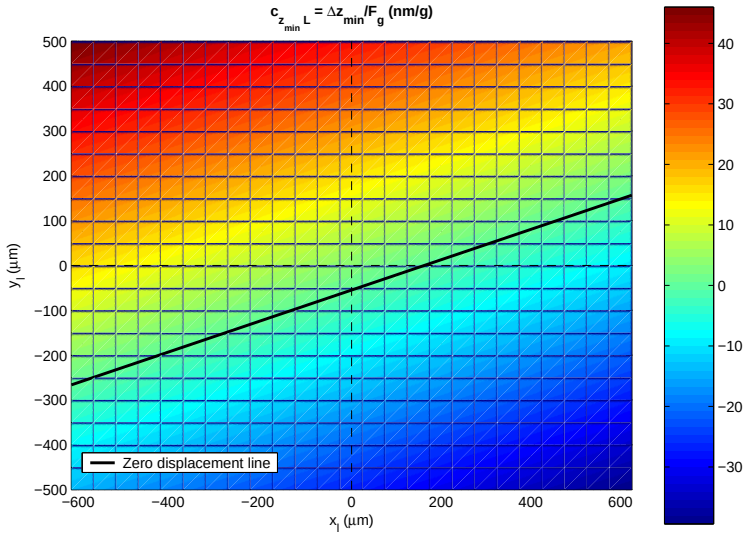

Figure 9: $c_{z_{min}G}$ variation along x_l and y_l

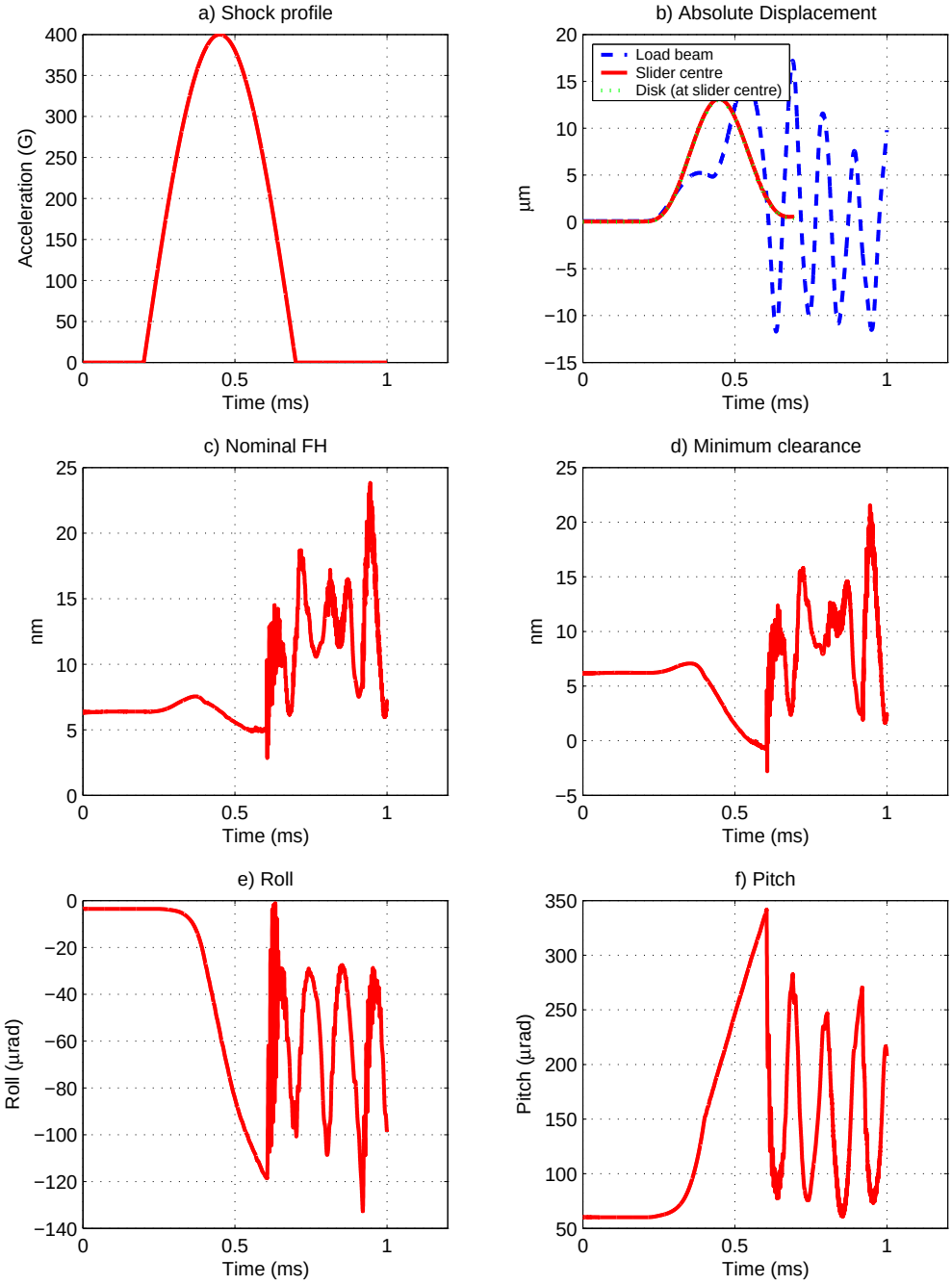

Figure 10: Slider attitude for U2 400G shock

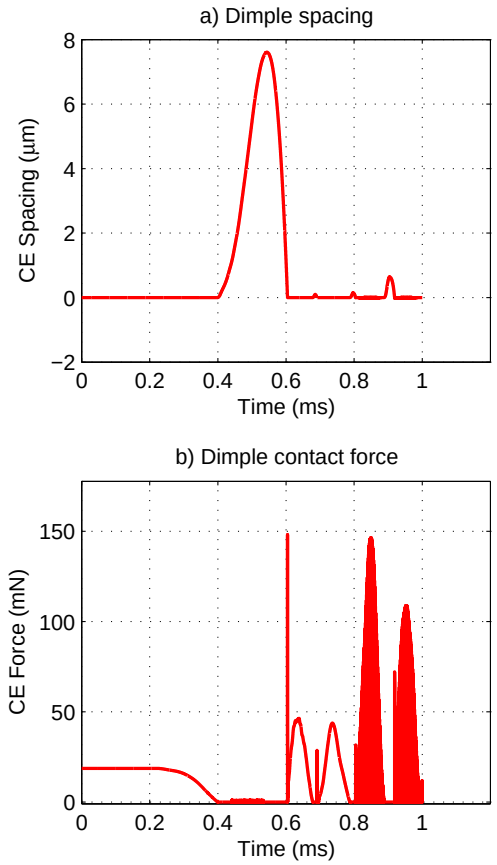

Figure 11: Dimple separation and contact force for U2 400G shock

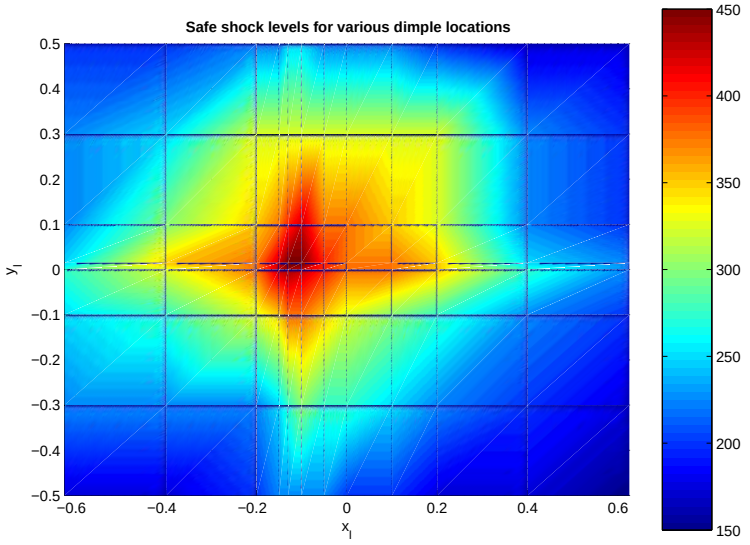

Figure 12: Safe shock levels for various dimple locations